



## RESEARCH ARTICLE

10.1029/2019EA001009

# Superiority of Mega-ENSO Index in the Seasonal Prediction of Tropical Cyclone Activity Over the Western North Pacific

## Key Points:

- The relative-SST-dependent mega-ENSO exhibits a higher skill in the seasonal forecasting compared with the absolute-SST-dependent ENSO
- More attention should be paid to the TCs in low mega-ENSO (La Niña) years which are more likely to occur in coastal areas
- Mega-ENSO contributes to migration of WNP TC exposure through its impact on TC genesis, TC potential intensity, and large-scale flow

Yuan Sun<sup>1,2</sup> , Zhong Zhong<sup>1,3</sup> , Tim Li<sup>2,4</sup> , Lan Yi<sup>5</sup>, Jian Shi<sup>1</sup>, Yixuan Shen<sup>1</sup>, Kefeng Liu<sup>1</sup> , Yijia Hu<sup>1</sup> , and Zanmin Xu<sup>2</sup>

<sup>1</sup>College of Meteorology and Oceanography, National University of Defense Technology, Nanjing, China, <sup>2</sup>Key Laboratory of Meteorological Disaster, Ministry of Education/Joint International Research Laboratory of Climate and Environmental Change/Collaborative Innovation Center on Forecast and Evaluation of Meteorological Disasters, Nanjing University of Information Science and Technology, Nanjing, China, <sup>3</sup>Jiangsu Collaborative Innovation Center for Climate Change, School of Atmospheric Sciences, Nanjing University, Nanjing, China, <sup>4</sup>IPRC and Department of Atmospheric Sciences, University of Hawai'i at Mānoa, Honolulu, HI, USA, <sup>5</sup>Academy of Meteorological Sciences/Chinese Meteorological Society, Beijing, China

## Correspondence to:

Z. Zhong,  
zhong\_zhong@yeah.net

## Citation:

Sun, Y., Zhong, Z., Li, T., Yi, L., Shi, J., Shen, Y., et al (2020). Superiority of mega-ENSO index in the seasonal prediction of tropical cyclone activity over the western North Pacific. *Earth and Space Science*, 7, e2019EA001009. <https://doi.org/10.1029/2019EA001009>

Received 21 NOV 2019

Accepted 16 APR 2020

Accepted article online 20 APR 2020

**Abstract** In this study, we compared the performance of two potential predictors, that is, El Niño–Southern Oscillation (ENSO) index (Niño-3.4) and mega-ENSO index, in the seasonal forecast of tropical cyclone (TC) activity and its spatial distribution over the western North Pacific (WNP) during the extended TC season, which is of public concern. Our results clearly show that, although both mega-ENSO and Niño-3.4 indices in the preceding May are important predictors for the seasonal prediction, the relative-sea surface temperature (SST)-dependent mega-ENSO exhibits a higher skill in the seasonal forecasting compared with the absolute-SST-dependent ENSO. Further results show that, despite of stronger destructiveness of TCs in high mega-ENSO (El Niño) years than in low mega-ENSO (La Niña) years, more attention should be paid to the TCs in low mega-ENSO years, which are more likely to occur in coastal areas compared with the TCs in high mega-ENSO years. Due to the responses of TC genesis, TC potential intensity, and large-scale flow to the SST change in low mega-ENSO years, the WNP TCs tend to originate in the northwestern quadrant and intensify at high latitudes and then turn northwestward over the TC prevailing region, which contributes to the northwestward migration of the WNP TC exposure in terms of track density and destructiveness density and thus imposes more risks in the coastal areas in low mega-ENSO years. In addition, despite the significant prediction skill in forecasting TC activity when using mega-ENSO/Niño-3.4 as a single predictor, it is still far to predict reliable WNP activity, especially its spatial distribution, without considering other predictors.

## 1. Introduction

Tropical cyclones (TCs) are probably the most devastating natural hazards (Emanuel, 2005a; Peduzzi et al., 2012; Shen et al., 2018; Zhang et al., 2009, 2016). The bulk of research on TCs has focused on the dynamics of TC genesis (Chia & Ropelewski, 2002; Gray, 1998), landfall (Chan & Liang, 2003; Kossin, 2018; Tuleya et al., 1984), track (Fraedrich & Leslie, 1989; Harr & Elsberry, 1991; Holland & Lander, 1993; Riehl & Shafer, 1944; Sun et al., 2017a), intensity (Camargo & Sobel, 2005; Emanuel et al., 2004), and destructiveness (Emanuel, 2005; Sun et al., 2017b). As the most active basin of TC frequency in the world (Chan, 2005), the TCs over the western North Pacific (WNP) cause serious social and economic destruction in the Asia-Pacific region (Gao et al., 2018; Park et al., 2011; Peduzzi et al., 2012). A skillful seasonal prediction of TC activities is crucial for the preparation and reduction of TC-related losses (Choi et al., 2016). Most seasonal TC prediction approaches target the location of cyclogenesis and the total number of TCs in the WNP (e.g., Camargo et al., 2007; Chan et al., 1998; Chia & Ropelewski, 2002). Some recent studies also examined predictability of TC track and intensity (Choi et al., 2016; Chu et al., 2007). However, not many studies were carried out on the seasonal prediction of TC activity and its spatial distribution, which are comprehensive predictands of public concern as they have significant impacts on the TC land-falling activities along the coastal areas of East Asia (Emanuel, 2005; Liu & Chan, 2008).

©2020 The Authors.

This is an open access article under the terms of the Creative Commons Attribution-NonCommercial License, which permits use, distribution and reproduction in any medium, provided the original work is properly cited and is not used for commercial purposes.

Based on the time-lag relationship between TC activities and precursory environmental conditions, a number of statistical models have been developed for seasonal predication of TC activities (e.g., Choi et al., 2016; Elsner & Jagger, 2006; Gray et al., 1992; Klotzbach, 2007; LaRow et al., 2010; Lehmiller et al., 1997). Some of these models have shown useful skills and have been employed in operational TC predictions. Determining the predictors is the prerequisite to the seasonal prediction of TC activities and directly affects the forecasting skill of these models. Climate variability on the interannual time scale is mainly driven by the circulation changes associated with the El Niño–Southern Oscillation (ENSO) (Aiyyer & Thorncroft, 2011; Chan & Zhou, 2005; Zhou & Chan, 2007). ENSO is a coupled atmosphere–ocean mode reflecting the interannual climate variability of tropical Pacific, and it provides a major source of seasonal TC predictability in the WNP (Camargo & Sobel, 2005; Chan & Yip, 2003; Li & Zhou, 2012; Patricola et al., 2018).

The scientific community has provided bulk of observational evidence supporting the influence of ENSO on TC genesis (Camargo et al., 2007; Chan, 1985; Fudeyasu et al., 2006; Wang et al., 2007; Wang & Chan, 2002), track (Camargo et al., 2007; Hong et al., 2011; Wang & Chan, 2002), intensity (Camargo & Sobel, 2005; Chan, 2008; Zhang et al., 2015), and landfall (Fudeyasu et al., 2006; Wu et al., 2004; Zhang et al., 2012) in the WNP. Most of these studies focused either on the relationship between TC activity and ENSO in TC prevailing seasons or on the predication of TC activity using ENSO in winter when ENSO signal is strong. However, the winter season may not be the most appropriate season for the ENSO as a predictor in predicting TC activity. As suggested by Wu et al. (2011), the net air–sea heat flux anomalies over the central tropical Pacific and the North Indian Ocean in the preceding season (e.g., April–June) are associated with ENSO and may be important contributors to TC activity in the WNP. Moreover, very few studies tried to associate TC activity and its spatial distribution with ENSO, let alone the seasonal predictability of TC activity and its spatial distribution using ENSO as a predictor. Furthermore, there are enormous studies investigating the impact of ENSO on WNP TC activity, but few have looked at the contributions of the other indices on interannual time scale.

A relatively new index, the mega-ENSO, is defined as the sea surface temperature (SST) difference between the western Pacific K-shape area and eastern Pacific triangle (see Figure 3 in Wang et al., 2013). As shown in Wang et al. (2013), the mega-ENSO is a multi–time scale index, which is not only highly correlated with the ENSO index on the interannual time scale but also well correlated with the Pacific Decadal Oscillation (Mantua et al., 1997) and Interdecadal Pacific Oscillation (Parker et al., 2007; Power et al., 1999) on the decadal and interdecadal time scales. Note that, in this study, similar to the Pacific Decadal Oscillation and Interdecadal Pacific Oscillation, the mega-ENSO also includes the extratropical SST signal, because besides the tropical SST, the extratropical SST also plays an important role in modulating the WNP TC activity (Aiyyer & Thorncroft, 2011; Chan, 2008; Hu et al., 2018; Kossin et al., 2016; Liu & Chan, 2008; Song & Klotzbach, 2018). Although the spatial pattern of mega-ENSO is similar to that of ENSO, it is not only with a larger spatial scale and a longer time scale but also determined by the relative value of SST rather than the absolute value of SST (Bamston et al., 1997; Webster et al., 1998; Wang et al., 2013). As indicated by previous studies, the changes in TC activity (e.g., TC frequency, intensity, and size) are controlled not by the absolute SST, but the relative SST (Chavas et al., 2016; Lee et al., 2018; Lin et al., 2015; Ramsay & Sobel, 2011; Swanson, 2008; Tippett et al., 2011; Vecchi et al., 2008; Vecchi & Soden, 2007). Thus, the mega-ENSO is expected to play an important role in determining TC activity and its spatial distribution over the WNP. Rather than developing a seasonal TC prediction model, the objective of this study is to examine the importance of ENSO or mega-ENSO index as a predictor in predicting TC activity and its spatial distribution over the WNP, including the latitudinal and longitudinal migrations of strong destructive potential areas, which are of great interest to the public.

## 2. Materials and Methods

The materials and methods parallel those of Sun et al. (2018) as follows in these paragraphs. The period of 1980–2016 is chosen in this study, in which the best track data are of high quality in terms of both storm location and intensity thanks to the geostationary satellites (Kossin et al., 2014; Sun et al., 2018). For the WNP TCs, there are four best track data sets from four different agencies: the Joint Typhoon Warning Center, the Japan Meteorological Agency, the China Meteorological Administration, and the Hong Kong Observatory. The SST data are from the U.S. National Oceanic and Atmospheric Administration (NOAA) Extended Reconstruction of SST (NOAA-ERSST; Smith & Reynolds, 2003), which is a global gridded

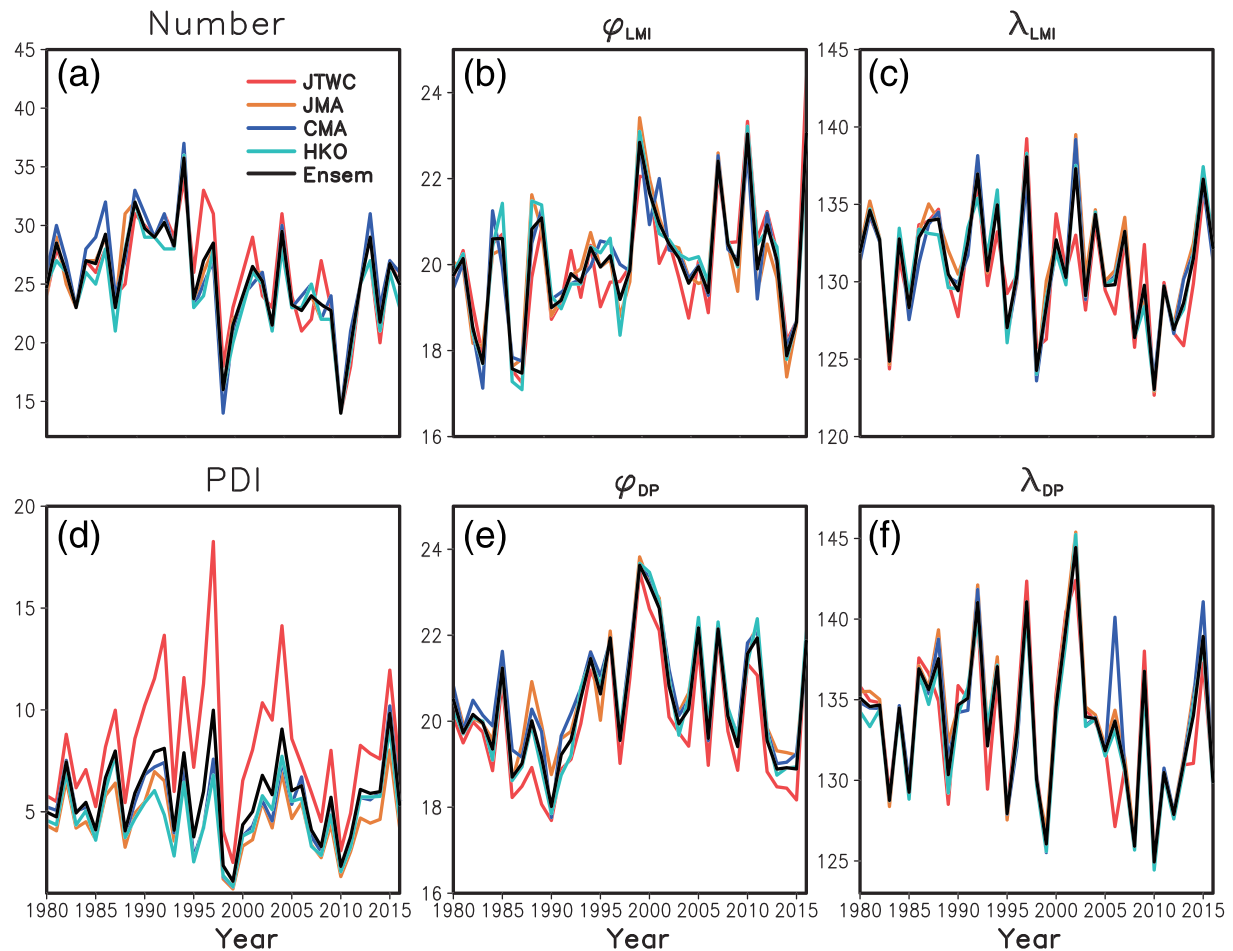


**Figure 1.** Time series of (a) annual TC number, (b, c) annual mean latitude ( $^{\circ}$ N) and longitude ( $^{\circ}$ E) of LMI ( $\varphi_{LMI}$  and  $\lambda_{LMI}$ ), (d) annual TC PDI, and (e, f) latitude ( $^{\circ}$ N) and longitude ( $^{\circ}$ E) weighted by TC destructive potential ( $\varphi_{DP}$  and  $\lambda_{DP}$ ) over the WNP calculated from various best track historical data sets.

reconstructed data set based on historical observed SST data using statistical methods. Monthly index of ENSO (Niño-3.4) is provided by NOAA's Earth System Research Laboratory Physical Sciences Division (Rayner et al., 2003; available at [http://www.esrl.noaa.gov/psd/gcos\\_wgsp/Timeseries/](http://www.esrl.noaa.gov/psd/gcos_wgsp/Timeseries/)). Temperature, pressure, humidity, and wind data are obtained from the National Centers for Environmental Prediction reanalysis data set (Kalnay, 1996), with a resolution of  $2.5^{\circ} \times 2.5^{\circ}$ .

### 3. Results

#### 3.1. Reliable Measurements to Detect the Migration of TC Activity

Previous studies suggested that the measurements of TC location (latitude and longitude) at the time of lifetime maximum intensity (LMI), that is,  $\varphi_{LMI}$  and  $\lambda_{LMI}$ , are expected to be comparatively robust due to the heterogeneity introduced into the best track data, by not only interagency procedural differences but also temporal inconsistency in data quality and analysis (Kossin et al., 2014, 2016; Sun et al., 2018). However, a recent study showed that these LMI metrics are not as certain as expected (Sun et al., 2018). Figures 1a–1c illustrate the time series of annual TC number, and annual mean  $\varphi_{LMI}$  and  $\lambda_{LMI}$ . Similar to the notable difference in annual TC number (Figure 1a), there are relatively large differences in both  $\varphi_{LMI}$  and  $\lambda_{LMI}$  among the various best track data sets (Figures 1b and 1c), with the standard deviations of  $0.47^{\circ}$  and  $1.15^{\circ}$ , respectively. So  $\varphi_{LMI}$  and  $\lambda_{LMI}$  are not as certain as expected, due to the uncertainties in both annual TC number and the moment when a TC reached its LMI according to these best track data sets. To reliably detect the meridional migration of TCs, Sun et al. (2018) recently designed a new metric, the

lifetime-averaged latitude weighted by TC destructive potential ( $\varphi_{DP}$ ), namely,  $\lambda_{DP}$ . Identical to the designing concept of  $\varphi_{DP}$ ,  $\lambda_{DP}$  is designed to detect the zonal shift of TC. The description of the two new metrics ( $\varphi_{DP}$  and  $\lambda_{DP}$ ) is identical to that of our previously published article (Sun et al., 2018), and the following text is derived from there with minor modifications. Apart from uncertain factors, these new metrics also consider public concerns (i.e., TC destructive potential). The destructive potential can be estimated by integration of the cube of maximum wind speed over its lifetime (i.e., power dissipation index or PDI; Emanuel, 2005). Thus,  $\varphi_{DP}$  and  $\lambda_{DP}$  of a TC and annually averaged  $\varphi_{DP}$  and  $\lambda_{DP}$  are given as follows:

$$\varphi_{DP} = \frac{\int_0^{\tau} \varphi \cdot V_{\max}^3 dt}{\int_0^{\tau} V_{\max}^3 dt} = \frac{\int_0^{\tau} \varphi \cdot V_{\max}^3 dt}{\text{PDI}} \quad (1)$$

$$\varphi_{DP\text{-annual}} = \frac{\sum_1^N (\varphi_{DP} \cdot \text{PDI})}{\sum_1^N \text{PDI}} = \frac{\sum_1^N \int_0^{\tau} \varphi \cdot V_{\max}^3 dt}{\sum_1^N \int_0^{\tau} V_{\max}^3 dt} \quad (2)$$

$$\lambda_{DP} = \frac{\int_0^{\tau} \lambda \cdot V_{\max}^3 dt}{\int_0^{\tau} V_{\max}^3 dt} = \frac{\int_0^{\tau} \lambda \cdot V_{\max}^3 dt}{\text{PDI}} \quad (3)$$

$$\lambda_{DP\text{-annual}} = \frac{\sum_1^N (\lambda_{DP} \cdot \text{PDI})}{\sum_1^N \text{PDI}} = \frac{\sum_1^N \int_0^{\tau} \lambda \cdot V_{\max}^3 dt}{\sum_1^N \int_0^{\tau} V_{\max}^3 dt} \quad (4)$$

where  $\tau$  is the lifetime of TC,  $V_{\max}$  is the maximum surface wind speed, and  $\varphi$  and  $\lambda$  are the latitude and longitude, respectively, of the TC center. To consider the contribution of weak TCs, the PDI definition used in this study is somewhat different from the PDI definition in Emanuel (2005), as ours considers all wind speeds while Emanuel's only considers the wind speed exceeding 17 m/s in the best track data set.

Figures 1d–1f show annual TC PDI, and annual mean  $\varphi_{DP}$  and  $\lambda_{DP}$ . Consistent with the results of Chan (2007), there are relatively large difference in PDI values among the four best track data sets because of large difference in data availability and operational techniques when estimating TC intensity among the four best track data sets (Figure 1d). Despite of large uncertainty in PDI,  $\varphi_{DP}$  and  $\lambda_{DP}$  are reliable measurements when there are relatively small differences in both  $\varphi_{DP}$  and  $\lambda_{DP}$  among the four best track data sets (Figures 1e and 1f), with the standard deviations of  $0.40^\circ$  and  $0.97^\circ$ , respectively, which are smaller than those of  $\varphi_{LMI}$  and  $\lambda_{LMI}$  ( $0.47^\circ$  and  $1.15^\circ$ ). As stated in Sun et al. (2018), this is because  $\varphi_{DP}$  and  $\lambda_{DP}$  consider the whole lifetime of TC rather than an instantaneous moment, and thus are not sensitive to the usual temporal heterogeneity of intensity estimate, the moments of cyclogenesis and cyclolysis, and the estimate of weak TC number, which are all relatively uncertain among the various best track data sets. More details on the reasons can be found in Sun et al. (2018). Overall,  $\varphi_{DP}$  and  $\lambda_{DP}$  are less sensitive to heterogeneity in the best track data sets than  $\varphi_{LMI}$  and  $\lambda_{LMI}$  and thus are more reasonable and reliable metrics in detecting meridional and zonal shifts of TCs, especially the meridional and zonal migrations of TC activity (Figure 1).

### 3.2. Seasonal Predictability of TC Activity and Its Spatial Distribution Using ENSO or Mega-ENSO Index as Predictor

Figure 2 shows the long-term distribution of monthly TC number and PDI in the WNP from 1980 to 2016. For these past decades, the observed WNP TCs are concentrated in the extended TC season from June to November, which accounts for 84.8% of the annual TC number and 87.8% of the annual TC PDI (Figure 2). Kim et al. (2017) also shown that, the 5th to 95th percentile of the TC formation dates properly occurred from June to November, which is known as the active TC season in the WNP. Thus, it is of public concern to predict the TC activity during the extended TC season.

TC activity on a seasonal time scale is modulated by large-scale environmental conditions (e.g., Gray, 1977; Watterson et al., 1995). In this study, we examine the importance of ENSO/mega-ENSO as a predictor in predicting TC activity and its spatial distribution over the WNP, including latitudinal and longitudinal migrations of strong destructive potential area. In the following, lagged correlation analysis is used to identify physical relationships (Sheng et al., 2020; Zhao et al., 2019). Figure 3 shows the lagged correlations between seasonal WNP TC activities (i.e., June–November TC number,  $\varphi_{LMI}$ ,  $\lambda_{LMI}$ , PDI,  $\varphi_{DP}$ , and  $\lambda_{DP}$ ) with Niño-3.4

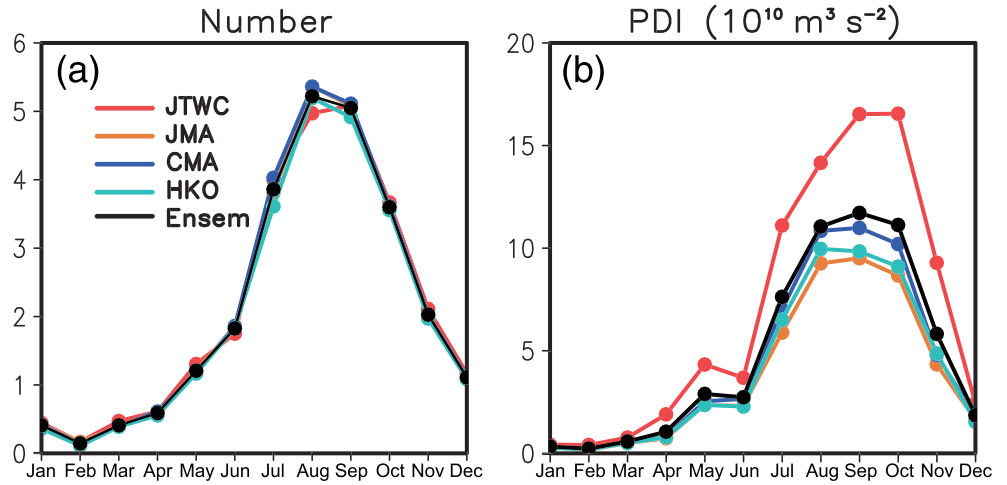


Figure 2. Long-term distributions of monthly TC number (a) and PDI (b) in the WNP from 1980 to 2016.

in different months. Consistent with previous studies (Camargo & Sobel, 2005; Chan, 1985), TC number is not significantly correlated with the ENSO index (i.e., Niño-3.4), and June–November TC number is more relevant to the Niño-3.4 in the preceding winter (e.g., December of year  $-1$ ) rather than that in the simultaneous June–November (of Year 0). Besides the high significant values of simultaneous correlations

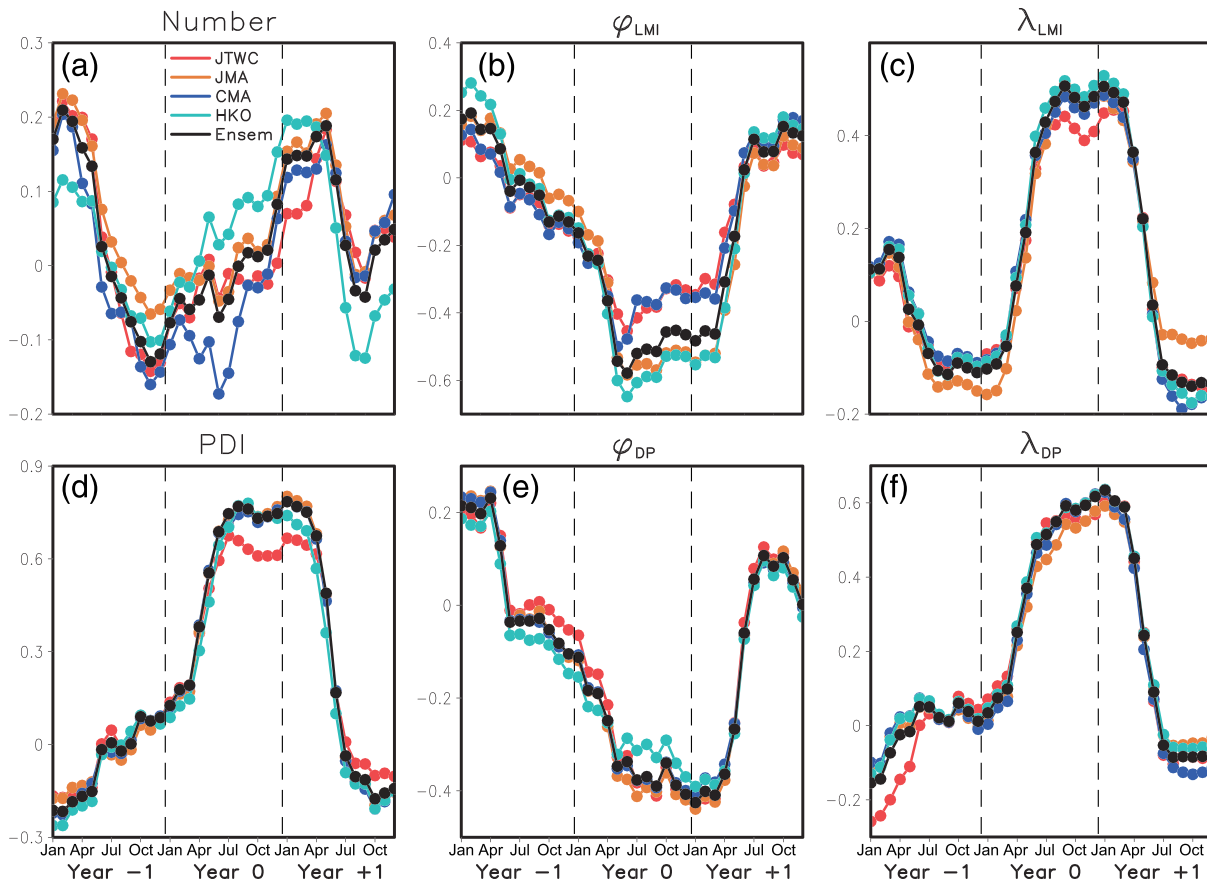
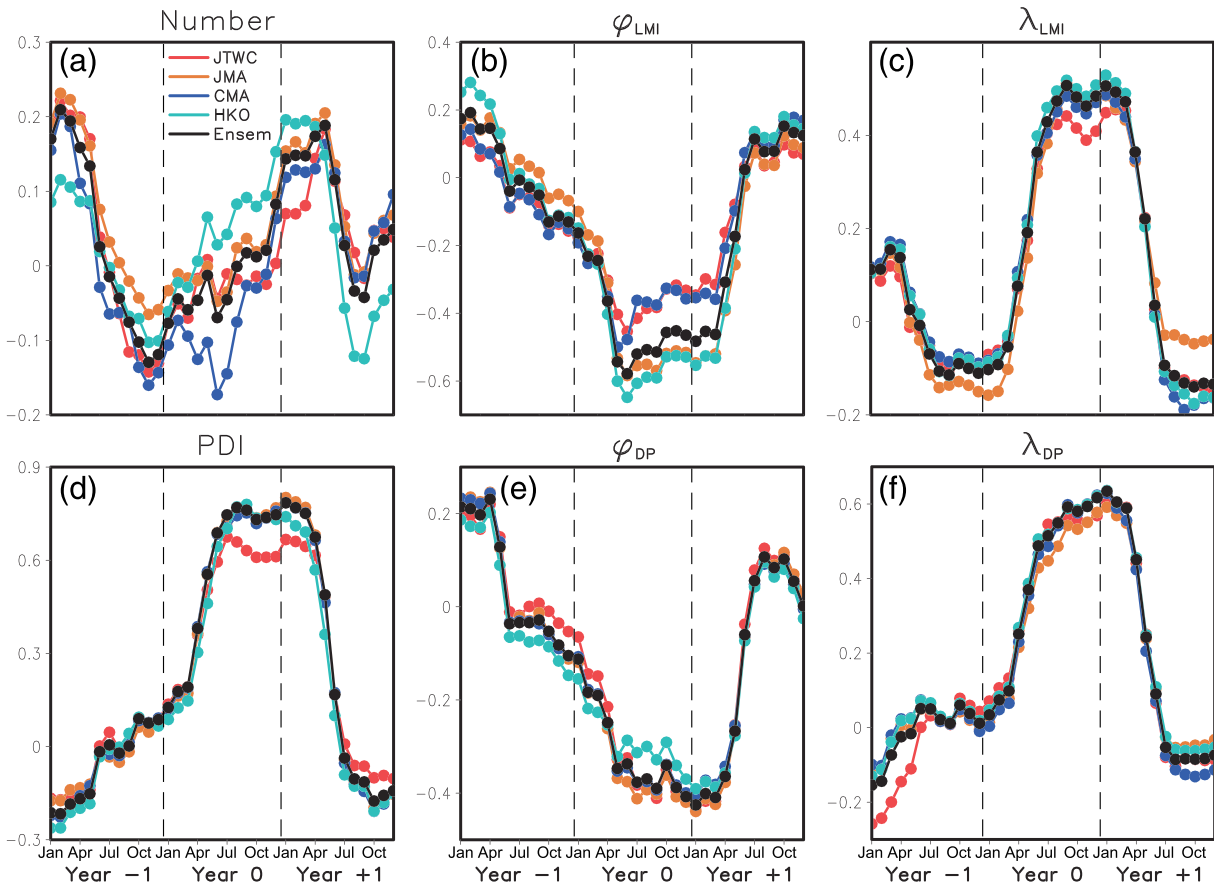


Figure 3. Lag correlations of time-averaged variables (i.e., [a] TC number, [b]  $\varphi_{LMI}$ , [c]  $\lambda_{LMI}$ , [d] PDI, [e]  $\varphi_{DP}$ , and [f]  $\lambda_{DP}$ ) during the extended TC season (June–November) with Niño-3.4 for different months.



**Figure 4.** Same as Figure 3 except for the lagged correlations of variables with mega-ENSO index.

(June–November of Year 0) of the other TC activities (i.e.,  $\varphi_{LMI}$ ,  $\lambda_{LMI}$ , PDI,  $\varphi_{DP}$ , and  $\lambda_{DP}$ ) with Niño-3.4, significant correlations start as early as May of Year 0 except for  $\lambda_{LMI}$  with Niño-3.4. Specifically, there is an inverse relationship between  $\varphi_{LMI}$  and Niño-3.4, especially for the Niño-3.4 in May, which is significant above the 95% confidence level. This indicates the ENSO contributes significantly to the latitudinal migration of WNP TCs in terms of latitude of LMI. However, there is no significant correlation between Jun–Nov  $\lambda_{LMI}$  and Niño-3.4 in May of Year 0. On the other hand, there is strong lag relationship between PDI and Niño-3.4 in the preceding May of Year 0, which is significant at the 99.9% confidence level. This is similar but not identical to the results of Camargo and Sobel (2005), which emphasized a significant and immediate relationship between the accumulated cyclone energy and ENSO in peak TC season (July–October). More importantly, the ENSO in May of Year 0 is also significantly correlated with June–November  $\varphi_{DP}$  and  $\lambda_{DP}$  (above the 95% confidence level). These results show that the ENSO index (i.e., Niño-3.4) is an important predictors in predicting not only TC activity (e.g., PDI) but also its spatial distribution over the WNP (e.g.,  $\varphi_{DP}$  and  $\lambda_{DP}$ ).

As Figure 3, Figure 4 shows the lagged correlations between seasonal WNP TC activities with mega-ENSO index in different months. Since the mega-ENSO index is highly correlated with the ENSO index on the interannual time scale (Wang et al., 2013), the patterns of lagged correlations with the mega-ENSO index are highly similar to those with the ENSO index, that is, the June–November TC number is more relevant to the mega-ENSO in the preceding winter, while the other June–November TC activities (i.e.,  $\varphi_{LMI}$ ,  $\lambda_{LMI}$ , PDI,  $\varphi_{DP}$ , and  $\lambda_{DP}$ ) are all simultaneously correlated with the mega-ENSO index. More importantly, the lagged correlations with the mega-ENSO are all higher than those with the ENSO in Year 0, especially in May of Year 0 (Figures 3 and 4). Specifically, the lagged correlation between June and November TC number with the mega-ENSO index nearly reaches 0.4 (Figure 4a), which is statistically significant and much larger

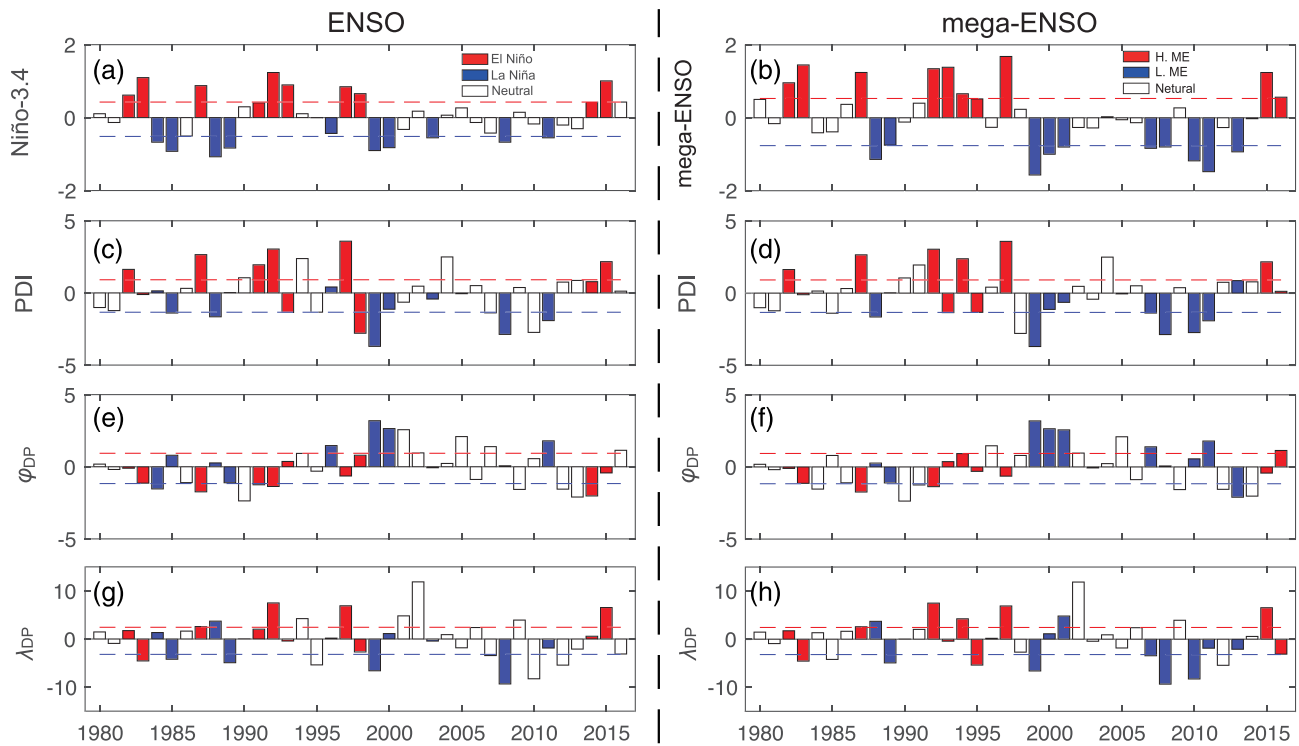


**Figure 5.** Relationship between ENSO/mega-ENSO in the preceding May and the TC activity, and their spatial distributions for the extended TC season (June–November). (a, b) Niño-3.4/mega-ENSO anomaly in the preceding May; (c, d) PDI anomaly for the extended TC season; (e and f)  $\varphi_{DP}$  and  $\lambda_{DP}$  anomalies for the extended TC season. The horizontal lines show the 25th percentile (blue dashed line) and 75th percentile (red dashed line).

than the nonsignificant lagged correlation with the ENSO index in the preceding May (Figure 3a). Moreover, the lagged correlations between June and November TC activities (i.e.,  $\varphi_{LMI}$ ,  $\lambda_{LMI}$ , PDI,  $\varphi_{DP}$ , and  $\lambda_{DP}$ ) with the mega-ENSO is about 0.05–0.10 larger than those with the ENSO index in the preceding May (Figures 3b–3f and 4b–4f). This may be because that, different from the ENSO index depending on the absolute SST (Bamston et al., 1997; Webster et al., 1998), the mega-ENSO index relies on the relative SST (Wang et al., 2013), which plays a more important role in determining TC activities than the absolute SST (Lee et al., 2018; Ramsay & Sobel, 2011; Swanson, 2008; Tippett et al., 2011; Vecchi et al., 2008; Vecchi & Soden, 2007). These results strongly indicate that, compared with the ENSO index (i.e., Niño-3.4), the mega-ENSO index is a more important predictor in predicting TC activity and its spatial distribution over the WNP.

Consistent with the results of Pudov and Petrichenko (2001) and of Camargo and Sobel (2005), the WNP TCs can be used as an indicator to predict ENSO/mega-ENSO, due to the significant lagged correlations of some seasonal TC activities (i.e., June–November  $\varphi_{LMI}$ ,  $\lambda_{LMI}$ , PDI,  $\varphi_{DP}$ , and  $\lambda_{DP}$ ) of Year 0 and Niño-3.4 in January–March of Year +1. However, according to the results of Camargo and Sobel (2005), the ENSO state in July–October of Year 0 is a much better indicator for forecasting ENSO in January–March of Year +1. The same is true for the mega-ENSO. Thus, it may not be necessary to use the TCs to predict the ENSO/mega-ENSO; instead, we should focus on the predictability of TC activities by using the ENSO/mega-ENSO in the preceding months (e.g., May of Year 0) rather than on the predictability of ENSO/mega-ENSO by using TC activities in the preceding months.

To investigate the predictability of TC activities by using ENSO/mega-ENSO in the preceding May and compare the performances of the two potential predictors (ENSO and mega-ENSO indices), we use Figure 5 to show the relationship between ENSO/mega-ENSO in the preceding May and TC activity, as well as its spatial distribution for the extended TC season (June–November). In this study, according to the value of the Niño-3.4 index (Bamston et al., 1997) in the month of interest (i.e., May), we define the 10 years (approximately 25% of the 37-year period) with the largest (smallest) values of Niño-3.4 in May as El Niño (La

Niña) years; the other 17 years as neutral years (Figure 5a). Similarly, in terms of the value of the mega-ENSO index (Wang et al., 2013) in the preceding May, we define the 10 years that are below the 25th (75th) percentile of the 37-yr period with the smallest (largest) value of the mega-ENSO index in May as high (low) mega-ENSO years, and the other 17 years as neutral years (Figure 5b). Despite of the high similarity of the two indices (Wang et al., 2013), their classifications of the 37-yr period are notably different, namely, not all the El Niño (La Niña) years correspond to the high (low) mega-ENSO years, and vice versa (Figures 5a and 5b). As suggested by Camargo and Sobel (2005), this kind of definition could avoid using thresholds, which are sensitive to season and can have asymmetries between warm and cold events.

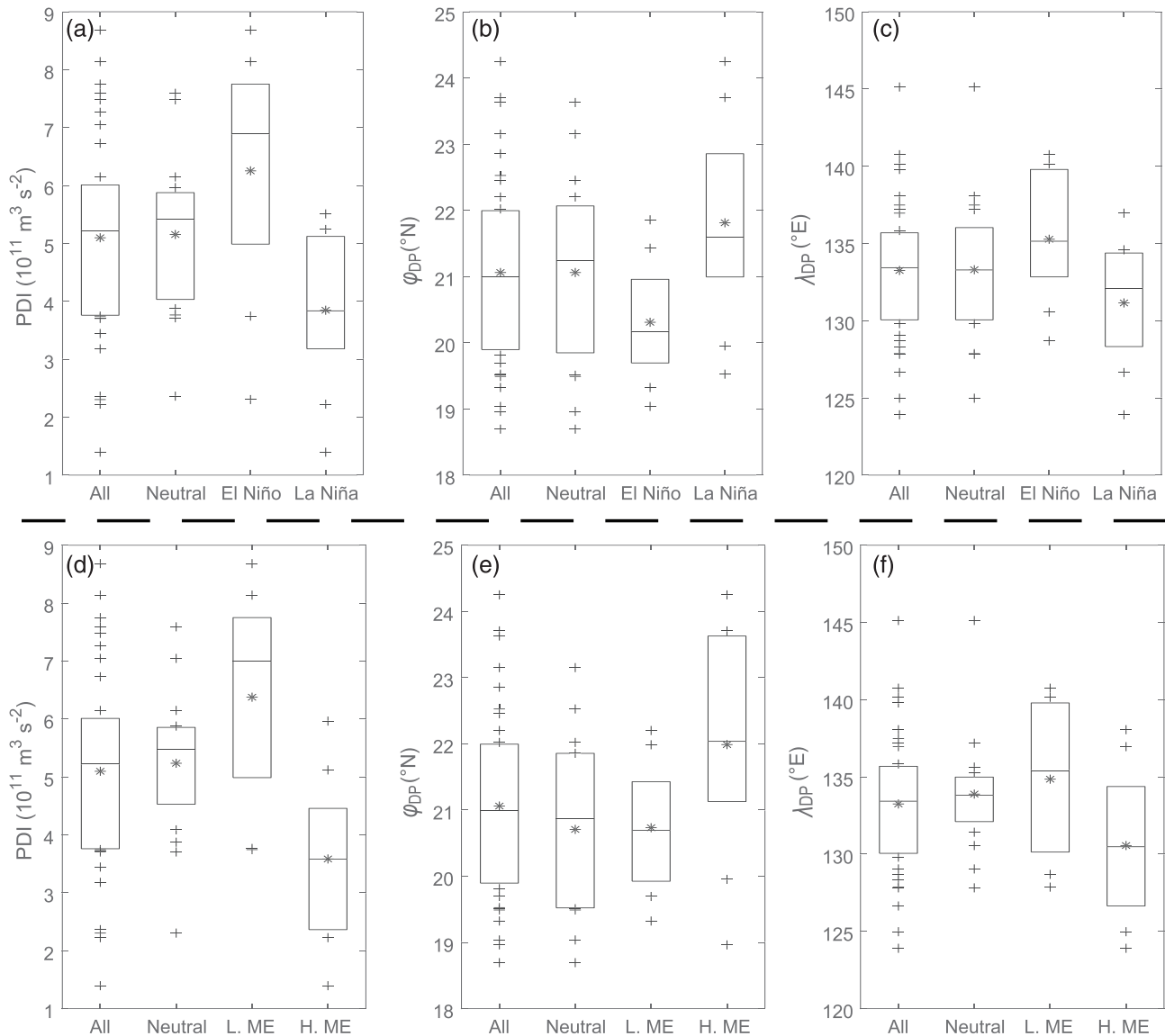
As shown in Figure 5c, the largest PDI value occurred in the extended TC season prior to the strongest El Niño year of the twentieth century, namely, 1997, while the year with the smallest PDI on record corresponded to a La Niña year (1999). This is consistent with years of the largest and smallest values of accumulated cyclone energy in Camargo and Sobel (2005). Of the 10 El Niño years, 7 have PDI values above the mean value of the period 1980–2016 (climatology), and 6 are above the 75th percentile of the climatology. On the contrary, seven of the 10 La Niña years have PDI values below the mean value of the climatology, and 5 of them are below the 25th percentile. Moreover, the locations weighted by TC destructive potential tend to occur in the southeast (northwest) region of the WNP in the El Niño years (Figures 4c and 4d). For  $\varphi_{DP}$  ( $\lambda_{DP}$ ), 7 of the 10 El Niño years are below (above) the mean value of the climatology, with 4 of them below the 25th percentile (above the 75th percentile), while 6 of the 10 La Niña years are above (below) the mean value, with 4 of them above the 75th percentile (below the 25th percentile). Similar results can be found in high/low mega-ENSO years, and there is a closer correspondence between mega-ENSO index and TC activity, as well as between their spatial distributions. Specifically, for the PDI, 6 of the 10 high (low) mega-ENSO years are above the 75th (below the 25th) percentile of the climatology, and none of them are below the 25th (above the 75th) percentile. For  $\varphi_{DP}$ , 3 (5) of the 10 high (low) mega-ENSO years are below the 25th (above the 75th) percentile, while for  $\lambda_{DP}$ , 5 of the 10 high (low) mega-ENSO years are above the 75th (below the 25th) percentile. Thereby, both ENSO and mega-ENSO in the preceding May are good indicators in forecasting not only TC activity but also its spatial distribution for the extended TC season. It seems that the mega-ENSO exhibits a better performance in seasonal forecasting, which will be confirmed in the last section.

To illustrate the relationship of the two indices with TC activity, as well as their spatial distributions, Figure 6 shows several characteristics of the distributions of PDI,  $\varphi_{DP}$ , and  $\lambda_{DP}$  (i.e., 25th and 75th percentiles, median, mean, and individual extreme values below (above) 25th (75th) percentiles), for different ENSO/mega-ENSO states from 1980 to 2016. Despite of the small sample size, significant differences between these distributions are evident. In El Niño (La Niña) years, the June–November PDI tends to be larger (smaller), and its spatial distribution is shifted in the southward (northward) and eastward (westward) directions (Figures 6a–6c). The differences of these variables (i.e., PDI,  $\varphi_{DP}$ , and  $\lambda_{DP}$ ) between El Niño and La Niña years are all statistically significant. Similar results can also be found in the differences of these variables among different mega-ENSO states (Figures 6d–6f).

Previous studies indicated that the TCs in El Niño years tend to be more intense and long-lived than those in La Niña years (e.g., Camargo, 2016; Camargo & Sobel, 2005; Patricola et al., 2018; Wang & Chan, 2002), which could explain the strong lagged relationship between the PDI and the ENSO. However, the underlying mechanisms on how the ENSO affects meridional and zonal migrations of TC activity are not yet revealed, let alone the mechanisms on the impact of the mega-ENSO, which will be discussed next.

### 3.3. Underlying Mechanisms for the Migration of TC Activity

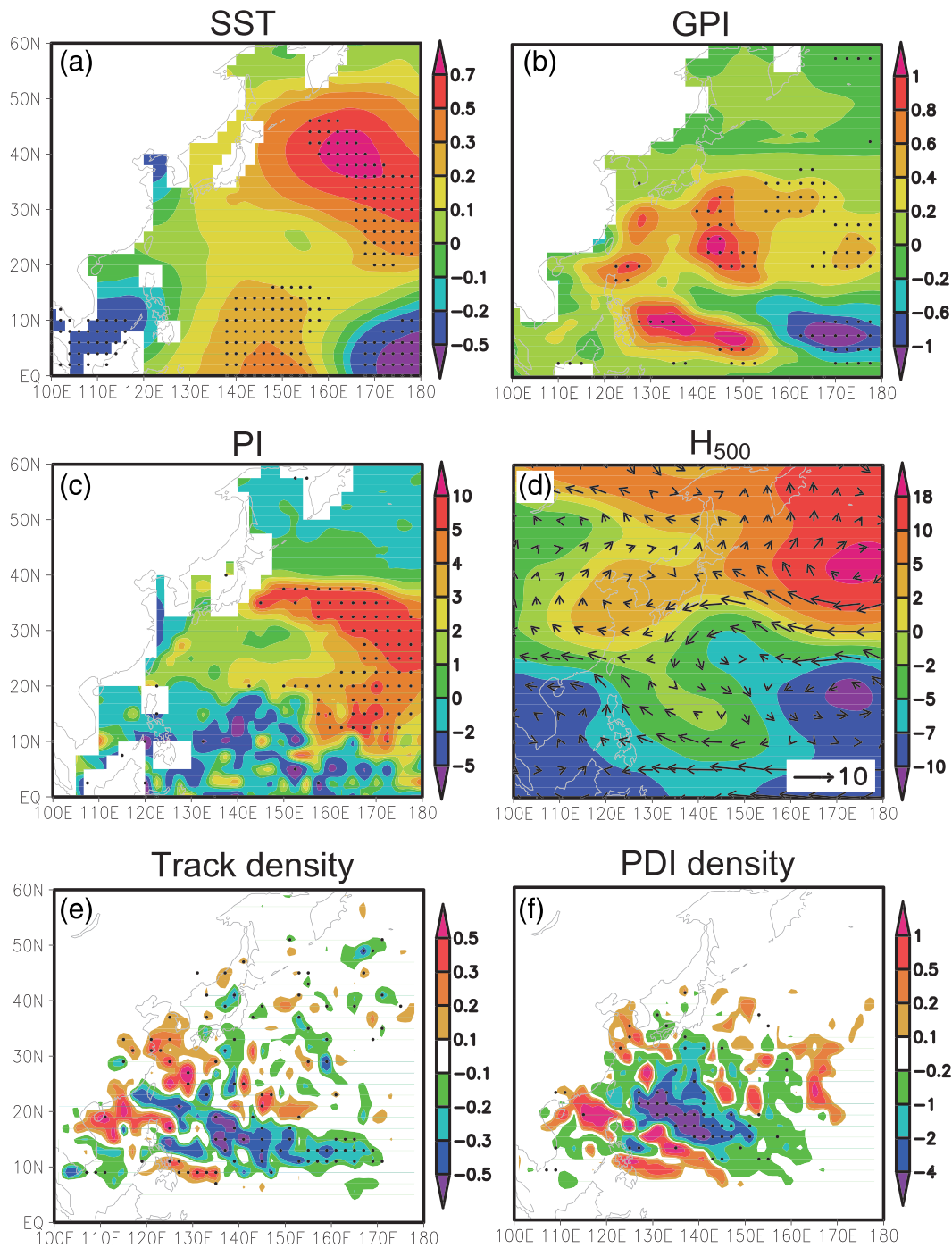
Migration of TC in terms of  $\varphi_{DP}$  and  $\lambda_{DP}$  is determined by TC genesis location, TC intensity evolution, and TC track pattern. The location is the starting position of a TC during its lifetime. TC intensity evolution shows when the high intensity occurs during its lifetime. TC track pattern describes the path of the TC, and thus illustrates where the high intensity might occur during its lifetime (He et al., 2020). In this study, these three factors are analyzed using the genesis potential index (GPI), potential intensity (PI), and large-scale environmental flow. The GPI is widely used to analyze spatial distribution of TC genesis potential and the influence of environmental factors on tropical cyclogenesis (Camargo et al., 2007). The PI can be considered as a major factor controlling TC intensity evolution (Emanuel, 1999), which describes the upper bound of intensity, which the environment will support and thus is closely associated with TC genesis and



**Figure 6.** Distributions of June–November (a, d) PDI, (b, e)  $\varphi_{DP}$ , and (c, f)  $\lambda_{DP}$  per year in all years, neutral years, El Niño (low mega-ENSO) years, and La Niña (high mega-ENSO) years, respectively. The boxes show the 25th and 75th percentiles, the line inside each box marks the median, the asterisks (\*) marks the mean, and the crosses mark the values below the 25th or above the 75th percentile of the distribution.

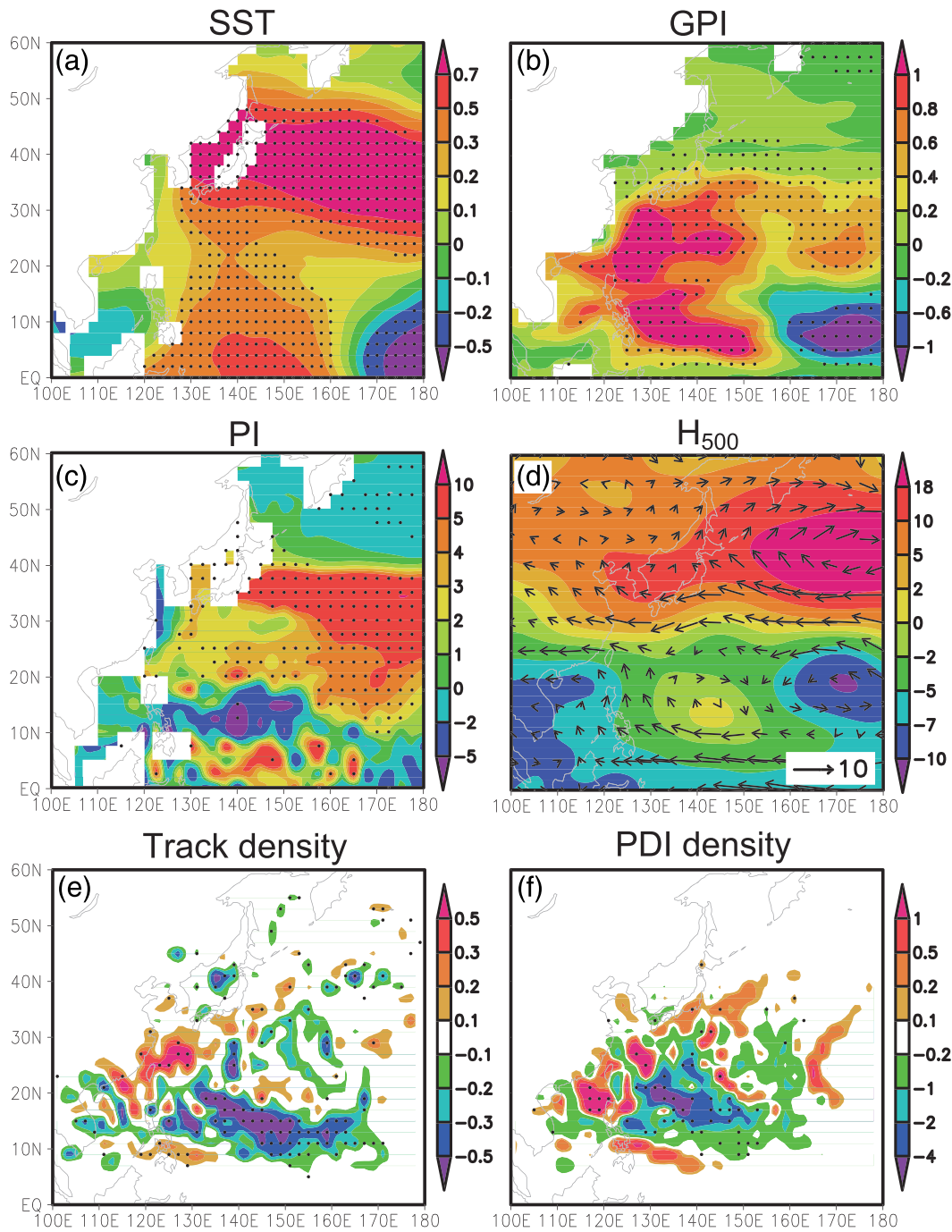
development. The large-scale environmental flow in the main TC activity region plays an important role in modulating the geographical properties of TC track over the WNP as TCs are usually steered by the surrounding flow (Chan & Gray, 1982; Sun et al., 2015). Therefore, the change of TC migration in terms of  $\varphi_{DP}$  and  $\lambda_{DP}$  can always be attributed to changes in the GPI, PI, and large-scale environmental flow. In this study, these three factors are all calculated using the National Centers for Environmental Prediction reanalysis data (Kalnay et al., 1996).

To our best knowledge, little is known about the impact of ENSO regional pattern on the migration of TC activity, let alone the impact of mega-ENSO regional pattern. The SSTs in El Niño and La Niña years (high and low mega-ENSO years) are characterized by different spatial distribution patterns. These patterns play important roles in determining the GPI and PI spatial distributions and the large-scale environmental flow in the main TC activity region (Camargo et al., 2007; Emanuel, 1999; Liu & Chan, 2008), which eventually affect the spatial distribution of TC activity in terms of  $\varphi_{DP}$  and  $\lambda_{DP}$ . Next, we will investigate the linkage of the migration of WNP TC activity with ENSO/mega-ENSO.



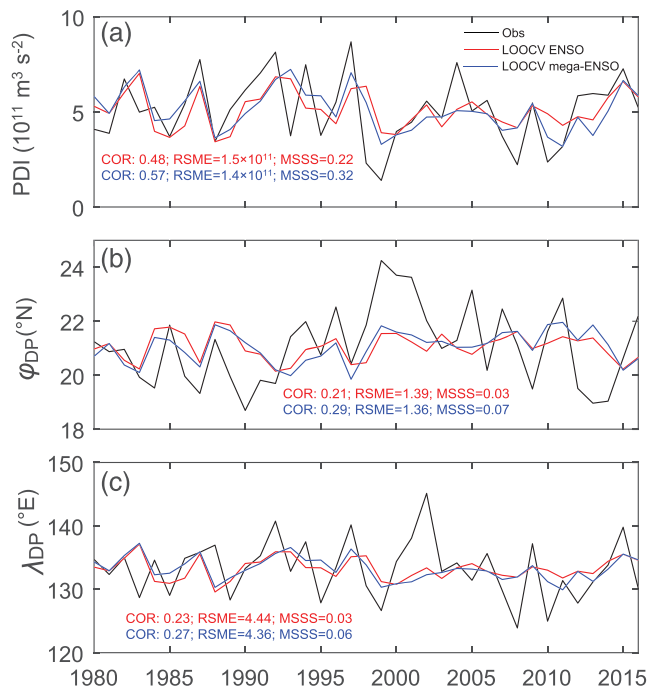
**Figure 7.** Differences in June–November SST, GPI, PI, large-scale circulation, and TC exposure between La Niña and El Niño years. (a) SST (°C); (b) GPI; (c) PI (m/s); (d) 500-hPa geopotential height (shading; m) and 850- to 300-hPa vertical mean wind (vector; m/s); (e) TC track density (number of days of exposure per year per  $2^\circ \times 2^\circ$  bin when a TC center is located in that bin); and (f) TC PDI density ( $10^9 \text{ m}^3/\text{s}^2$ ; accumulated PDI per year per  $2^\circ \times 2^\circ$  bin when a TC center is located in that bin). Stippling denotes that the difference is significant at or above the 95% (90%) confidence level by Student's  $t$  test in Figures 7a–7c (Figures 7e and 7f).

Figure 7 compares annual mean (June–November mean) differences of SST, GPI, PI, large-scale circulation, TC track density, and PDI density during the El Niño and La Niña years. Recall that El Niño and La Niña years are defined according to the value of the Niño-3.4 index in May in this study. Comparing the SSTs in La Niña years with those in El Niño years, there are three main regions (*northeast region*: 155–180°E,



**Figure 8.** Same as Figure 7 except for the differences between high and low mega-ENSO years.

20–45°N; *southwest region*: 135–160°E, 0–20°N; *southeast region*: 165–180°E, 0–10°N) where SST anomalies are significant at or above the 95% confidence level (Figure 7a). First, the changes of SSTs in these regions contribute to the remarkable change of GPI in the four ocean areas, that is, an ocean area south of Japan (120–150°E, 15–35°N), an ocean area near the central North Pacific (155–180°E, 20–35°N), and two ocean areas near the equator [(125–155°E, 0–10°N) and (160–180°E, 0–10°N)]. Compared with the area south of Japan, which is north of the main WNP TC genesis area, the other three areas are relatively farther away from the main TC genesis region over the WNP and thus contribute relatively less to the migration of TC genesis location (Figure 7b). Under the effect of GPI change in the area south of Japan, the time-averaged



**Figure 9.** Time series of June–November TC (a) PDI ( $10^{11} \text{ m}^3/\text{s}^2$ ), (b)  $\varphi_{DP}$  ( $^{\circ}\text{N}$ ), and (c)  $\lambda_{DP}$  ( $^{\circ}\text{E}$ ) from 1980 to 2016. The black line indicates observations, and red (blue) line shows LOOCV prediction based on the ENSO (mega-ENSO) index. The correlation coefficient (COR), root-mean-square error (RMSE), and mean square skill score (MSSS) of LOOCV prediction are also shown as annotated values (red values show ENSO results, and blue values show mega-ENSO results).

TC genesis location shifts poleward by  $1.91^{\circ}$  in latitude and westward by  $2.84^{\circ}$  in longitude. As suggested by previous studies, this could result in shorter-lived and weaker TCs in La Niña years than in El Niño years (Camargo & Sobel, 2005; Tu et al., 2018; Wang & Chan, 2002), which explains why smaller PDI is seen in La Niña years than in El Niño years. Moreover, the higher SST in the *northeast region* induces a higher PI that contributes to the further development of TCs in the higher latitudes near the region (Figure 7c) and eventually favors the poleward shift of TC activity in terms of  $\varphi_{DP}$ . More importantly, the higher SST in the *southwest region* contributes to positive geopotential height anomalies in this region as ocean warming is favorable for the development of the deep, warm high (i.e., the western Pacific subtropical high or the WPSH) in the off-equatorial region ( $>5^{\circ}\text{N}$ ), which leads to the westward expansion of the WPSH over the *southwest region* (Figure 7d). The anticyclonic anomaly in the western boundary of the westward expanded WPSH contributes to an increase in the northwestward steering flow over the TC prevailing region of ( $120\text{--}135^{\circ}\text{E}$ ,  $10\text{--}25^{\circ}\text{N}$ ), which tends to promote northwestward turning of westward moving TCs over the region (Figure 7d). In addition to the changes of  $\varphi_{DP}$  and  $\lambda_{DP}$ , the intensified northwestward steering flow, together with the changes of GPI and PI, also contribute to increases in TC track density and PDI density over the regions of the East China Sea, and many coastal areas (e.g., off Taiwan, Ryukyu Islands, Luzon, Hainan, and the southeastern coast of China) but decreases in TC track density and PDI density in large marine regions (e.g., western part of the WNP) and a few coastal areas (e.g., off Vietnam) (Figures 7e and 7f).

Figure 8 is the same as Figure 7, except for the differences between high and low mega-ENSO years. The spatial distribution patterns of the differences in Figure 8 are similar to those between El Niño and La Niña years (Figure 7) but with a larger magnitude. Both the magnitude and 95% significant area of SST differences between high and low mega-ENSO years are significantly larger than those between El Niño and La Niña years (Figures 7a and 8a). This leads to larger differences in GPI, PI, and large-scale circulation (Figures 7b–7d and 8b–8d) and eventually contributes to larger differences in TC track density and PDI density (Figures 7e, 7f, 8e, and 8f). This is consistent with our aforementioned assumption that while the ENSO index depends on the absolute SST (i.e., Niño-3.4), the mega-ENSO index depends on the relative SST (i.e., the SST difference between the western Pacific K-shape area and eastern Pacific triangle; Wang et al., 2013), which contributes more to the change of TC activity than the absolute SST (Chavas et al., 2016; Lee et al., 2018; Lin et al., 2015; Ramsay & Sobel, 2011; Swanson, 2008; Tippett et al., 2011; Vecchi et al., 2008; Vecchi & Soden, 2007) and thus is expected to play a more important role in determining WNP TC activity and its spatial distribution. Detailed mechanisms on the impact of mega-ENSO are similar to those on the impact of ENSO. Overall, due to the responses of GPI, PI, and large-scale flow to ENSO (mega-ENSO), the WNP TCs tend to originate in a northwestern region and intensify at the high latitudes and turn northwestward over the TC prevailing region, which contributes to the northwestward migration of the WNP TC track and destructiveness and thus imposes more risks in coastal areas despite of relatively smaller total PDI in La Niña (low mega-ENSO) years. Moreover, compared with the difference in SST between El Niño and La Niña years (Figure 7a), the SST difference between high and low mega-ENSO years is larger and more significant (Figure 8a). This causes larger differences in SST-induced GPI, PI, and large-scale environmental flow (Figures 8b–8d) and eventually leads to larger difference in TC activity between high and low mega-ENSO years (Figures 8e and 8f), compared with the differences between El Niño and La Niña years (Figures 7b–7f). This implies that the impact of mega-ENSO may be larger than the impact of ENSO on WNP TC activity.

#### 4. Conclusions and Discussion

The ENSO is a major source of seasonal TC predictability in several ocean basins, including the WNP, which have been well studied. However, less attention was paid to the contributions of the other indices on the interannual time scale. Different from previous studies, we focused on the impact of ENSO/mega-ENSO on WNP TC activity, especially its spatial distribution, and compare the performances of the two indices in the TC seasonal forecasting. We found that the June–November TC activity and its spatial distribution are closely related to the ENSO and mega-ENSO indices in the preceding May. This strongly suggests that the ENSO/mega-ENSO index in the preceding May is an important predictor for the seasonal predication of TC activity and its spatial distribution over the WNP, which are of great interest to the public. More importantly, compared with the ENSO index (i.e., Niño-3.4) determined by the absolute value of SST, the mega-ENSO index, which depends on the relative value of SST, can be considered as a more important predictor in predicting TC activity and its spatial distribution over the WNP. Moreover, different from the conclusions of previous studies, which indicated that TCs are more intense with longer lifetime and thus more destruction in El Niño years than in La Niña years (Camargo & Sobel, 2005; Tu et al., 2018), our results using the spatial distribution of TC activity show that more attention should be paid to the TC-induced damage in coastal areas in La Niña (low mega-ENSO) years than in El Niño (high mega-ENSO) years. Possible physical mechanisms are also revealed in this study. ENSO (mega-ENSO) related SST change induces changes of GPI, PI, and large-scale flow, which contributes to the northwestward migration of WNP activity and thus imposes more risks in coastal areas but less risks in open-ocean areas in La Niña (low mega-ENSO) years. Specifically, consistent with the results of some previous studies (Song & Klotzbach, 2018; Wu et al., 2012; Wu & Wang, 2004), the change of TC genesis location plays an important role in determining the change of spatial distribution of TC activity (e.g.,  $\varphi_{DP}$  and  $\lambda_{DP}$ ) due to the northwestward shift of TC genesis location. Moreover, the changes of PI and large-scale environmental flow also contribute greatly to the northwestward shift of TC activity. Furthermore, compared to the difference between La Niña and El Niño years, the difference in SST, GPI, PI, and large-scale environmental flow between low and high mega-ENSO years seem to be larger and more significant, thus leading to larger and more significant difference in TC activity between low and high mega-ENSO years. This also implies that, compared with the ENSO index, the mega-ENSO index may be a better predictor for forecasting WNP activities.

To further quantitatively compare the performance of two potential predictors (ENSO and mega-ENSO indices), it is proper to employ the leave-one-out-cross-validation (LOOCV) method, which is widely used to estimate the performance of statistical prediction (Choi et al., 2016; Chu & Zhao, 2007; Elsner & Schmertmann, 1993; Gray et al., 1992), due to the fact that the variation of TC activity is approximately independent from year to year. Specifically, in this study, when a target year is chosen, the model is iteratively adjusted using the remaining 37-year data as the training set. The observations of the selected predictor (i.e., the ENSO/mega-ENSO index in the preceding May) for the target year are then used as inputs to predict the target year. This process is repeated successively until all 37 forecasts are made. Figure 9 shows the time series of predicted June–November TC PDI,  $\varphi_{DP}$ , and  $\lambda_{DP}$  based on the ENSO/mega-ENSO index, together with observations. The correlation coefficient (COR), root-mean-square error (RMSE), and mean square skill score (MSSS) of the LOOCV predictions with the observations are shown in Figure 9. These measures are widely used to test the reliability of forecast (Choi et al., 2016; Wilks, 2006). As is shown in Figure 9a, the hindcast of TC PDI based on the ENSO (mega-ENSO) index is significantly correlated to observations above the 99.9% confidence level, with COR value exceeding 0.48 (0.57). This indicates that our simple LOOCV predication model using the ENSO or mega-ENSO index, especially the latter, as a single predictor can reliably reforecast the interannual variation of the observed TC PDI with several months in advance. The RMSE based on the ENSO/mega-ENSO index is relatively small, which accounts for about 30% of time-averaged TC PDI. The MSSS is the ratio of the mean square error of the forecast compared to that of the observation. The MSSS of PDI based on the ENSO or mega-ENSO index is significantly larger than 0, indicating that our simple model has significant predication skill compared to climatology-based reference forecasts in which the MSSS is equal to 0. On the other hand, the ENSO and mega-ENSO index all exhibits relatively lower skills in forecasting meridional and zonal migrations of strong TC destructive potential areas (i.e.,  $\varphi_{DP}$  and  $\lambda_{DP}$ ) (Figures 9b and 9c). Yet there are still some improvements in predicting  $\varphi_{DP}$  and  $\lambda_{DP}$  over climatology-based reference predictions as the MSSS values of predicted  $\varphi_{DP}$  and  $\lambda_{DP}$  are larger than 0. More importantly, our results clearly indicate that compared with the ENSO index, the mega-ENSO index

is a better predictor in forecasting TC activity (i.e., PDI) and its spatial distributions (i.e.,  $\varphi_{DP}$  and  $\lambda_{DP}$ ) in terms of all the metrics (i.e., COR, RMSE, and MSSS values). This may be because that compared with the absolute-SST-dependent ENSO index, the relative-SST-dependent mega-ENSO index is more relevant to changes of TC activities (e.g., destructiveness and its spatial distribution). Note that, due to the limited samples (1980–2016), it is hard to detect a significant difference in the absolute errors of TC activities (e.g., PDI,  $\varphi_{DP}$ , and  $\lambda_{DP}$ ) between the predictions based on the mega-ENSO index and those based on the ENSO index. In addition, we emphasize the importance of ENSO/mega-ENSO as a predictor for forecasting WNP TC activities (e.g., destructiveness and its spatial distribution) in this study. However, it does not mean that we can predict the WNP activities accurately by using ENSO/mega-ENSO as the sole predictor. Based on the forecast skills of our simple model using the ENSO or mega-ENSO index as a single predictor, it is difficult to anticipate reliable WNP TC activity and its spatial distribution without considering the other predictors. To improve the accuracy of the prediction model, we plan to not only find more effective predictors but also improve the prediction method and model for predicting seasonal TC activities over the WNP.

### Acknowledgments

This work is sponsored by the National Natural Science Foundation of China (Grants 41605072, 41430426, and 41675077) and the Natural Science Foundation of Jiangsu Province (Grant BK20160768). We thank Dr. Suzana J. Camargo for her valuable suggestions. The data used in this study can be downloaded at the website (<https://doi.org/10.5281/zenodo.3715531>).

### References

- Ayyer, A., & Thorncroft, C. (2011). Interannual-to-multidecadal variability of vertical shear and tropical cyclone activity. *Journal of Climate*, *24*, 2949–2962. <https://doi.org/10.1175/2010JCLI3698.1>
- Bamston, A. G., Chelliah, M., & Goldenberg, S. B. (1997). Documentation of a highly ENSO-related SST region in the equatorial Pacific. *Atmosphere-Ocean*, *35*, 367–383. <https://doi.org/10.1080/07055900.1997.9649597>
- Camargo, S. J. (2016). Tropical cyclones, western North Pacific basin [in “state of the climate in 2015”]. *Bulletin of the American Meteorological Society*, *97*, S110–S114. <https://doi.org/10.1175/2016BAMSStateoftheClimate.1>
- Camargo, S. J., Emanuel, K. A., & Sobel, A. H. (2007). Use of a genesis potential index to diagnose ENSO effects on tropical cyclone genesis. *Journal of Climate*, *20*, 4819–4834. <https://doi.org/10.1175/JCLI4282.1>
- Camargo, S. J., & Sobel, A. H. (2005). Western North Pacific tropical cyclone intensity and ENSO. *Journal of Climate*, *18*, 2996–3006. <https://doi.org/10.1175/JCLI3457.1>
- Chan, J. C. L. (1985). Tropical cyclone activity in the northwest Pacific in relation to the El Niño/Southern Oscillation phenomenon. *Monthly Weather Review*, *113*, 599–606. [https://doi.org/10.1175/1520-0493\(1985\)113<0599:TCAITN.2.0.CO;2](https://doi.org/10.1175/1520-0493(1985)113<0599:TCAITN.2.0.CO;2)
- Chan, J. C. L. (2005). Interannual and interdecadal variations of tropical cyclone activity over the western North Pacific. *Meteorology and Atmospheric Physics*, *89*, 143–152. <https://doi.org/10.1007/s00703-005-0126-y>
- Chan, J. C. L. (2007). Interannual variations of intense typhoon activity. *Tellus*, *59A*, 455–460.
- Chan, J. C. L. (2008). Decadal variations of intense typhoon occurrence in the western North Pacific. *Proceedings of the Royal Society of London*, *464A*, 249–272. <https://doi.org/10.1098/rspa.2007.0183>
- Chan, J. C. L., & Gray, W. M. (1982). Tropical cyclone movement and surrounding flow relationships. *Monthly Weather Review*, *110*, 1354–1374.
- Chan, J. C. L., & Liang, X. (2003). Convective asymmetries associated with tropical cyclone landfall. Part I: f-plane simulations. *Journal of the Atmospheric Sciences*, *60*, 1560–1576. [https://doi.org/10.1175/1520-0469\(2003\)60<1560:CAAWTC.2.0.CO;2](https://doi.org/10.1175/1520-0469(2003)60<1560:CAAWTC.2.0.CO;2)
- Chan, J. C. L., Shi, J. S., & Lam, C. M. (1998). Seasonal forecasting of tropical cyclone activity over the western North Pacific and the South China Sea. *Weather and Forecasting*, *13*, 997–1004. [https://doi.org/10.1175/1520-0434\(1998\)013<0997:TCO.2.0.CO;2](https://doi.org/10.1175/1520-0434(1998)013<0997:TCO.2.0.CO;2)
- Chan, J. C. L., & Yip, C. K. M. (2003). Interannual variations of tropical cyclone size over the western North Pacific. *Geophysical Research Letters*, *30*, 2267. <https://doi.org/10.1029/2003GL018522>
- Chan, J. C. L., & Zhou, W. (2005). PDO, ENSO and the early summer monsoon rainfall over South China. *Geophysical Research Letters*, *32*, L08810. <https://doi.org/10.1029/2004GL022015>
- Chavas, D. R., Lin, N., Dong, W., & Lin, Y. (2016). Observed tropical cyclone size revisited. *Journal of Climate*, *29*, 2923–2939. <https://doi.org/10.1175/JCLI-D-15-0731.1>
- Chia, H. H., & Ropelewski, C. (2002). The interannual variability in the genesis location of tropical cyclones in the Northwest Pacific. *Journal of Climate*, *15*, 2934–2944. [https://doi.org/10.1175/1520-0442\(2002\)015<2934:TIVITG.2.0.CO;2](https://doi.org/10.1175/1520-0442(2002)015<2934:TIVITG.2.0.CO;2)
- Choi, W., Ho, C.-H., Kim, J., Feng, S., & Kang, K. (2016). A track pattern-based seasonal prediction of tropical cyclone activity over the North Atlantic. *Journal of Climate*, *29*, 481–494. <https://doi.org/10.1175/JCLI-D-15-0407.1>
- Chu, P.-S., & Zhao, X. (2007). A Bayesian regression approach for predicting seasonal tropical cyclone activity over the central North Pacific. *Journal of Climate*, *20*, 4002–4013. <https://doi.org/10.1175/jcli4214.1>
- Chu, P.-S., Zhao, X., Lee, C.-T., & Lu, M.-M. (2007). Climate prediction of tropical cyclone activity in the vicinity of Taiwan using the multivariate least absolute deviation regression method. *Terrestrial, Atmospheric and Oceanic Sciences*, *18*, 805–825. [https://doi.org/10.3319/TAO.2007.18.4.805\(A\)](https://doi.org/10.3319/TAO.2007.18.4.805(A))
- Elsner, J. B., & Jagger, T. H. (2006). Prediction models for annual U.S. hurricane counts. *Journal of Climate*, *19*, 2935–2952. <https://doi.org/10.1175/JCLI3729.1>
- Elsner, J. B., & Schmertmann, C. P. (1993). Improving extended range seasonal predictions of intense Atlantic hurricane activity. *Weather and Forecasting*, *8*, 345–351. [https://doi.org/10.1175/1520-0434\(1993\)008<0345:IERSP.2.0.CO;2](https://doi.org/10.1175/1520-0434(1993)008<0345:IERSP.2.0.CO;2)
- Emanuel, K. (2005a). *Divine wind: The history and science of hurricanes*, (p. 296). Oxford: Oxford University Press.
- Emanuel, K., DesAutels, C., Holloway, C., & Korty, R. (2004). Environmental control of tropical cyclone intensity. *Journal of the Atmospheric Sciences*, *61*, 843–858. [https://doi.org/10.1175/1520-0469\(2004\)061<0843:ECOTCI.2.0.CO;2](https://doi.org/10.1175/1520-0469(2004)061<0843:ECOTCI.2.0.CO;2)
- Emanuel, K. A. (1999). Thermodynamic control of hurricane intensity. *Nature*, *401*, 665–669. <https://doi.org/10.1038/44326>
- Emanuel, K. A. (2005). Increasing destructiveness of tropical cyclones over the past 30 years. *Nature*, *436*(7051), 686–688. <https://doi.org/10.1038/nature03906>
- Fraedrich, K., & Leslie, L. M. (1989). Estimates of cyclone track predictability. I: Tropical cyclones in the Australian region. *Quarterly Journal of the Royal Meteorological Society*, *115*, 79–92. <https://doi.org/10.1002/qj.49711548505>

- Fudeyasu, H., Iizuka, S., & Matsuura, T. (2006). Impact of ENSO on landfall characteristics of tropical cyclones over the western North Pacific during the summer monsoon season. *Geophysical Research Letters*, 33, L21815. <https://doi.org/10.1029/2006GL027449>
- Gao, S., Zhu, L., Zhang, W., & Chen, Z. (2018). Strong modulation of the Pacific Meridional mode on the occurrence of intense tropical cyclones over the Western North Pacific. *Journal of Climate*, 31, 7739–7749. <https://doi.org/10.1175/JCLI-D-17-0833.1>
- Gray, W. M. (1977). Tropical cyclone genesis in the western North Pacific. *Journal of the Meteorological Society of Japan*, 55, 465–482.
- Gray, W. M. (1998). The formation of tropical cyclones. *Meteorology and Atmospheric Physics*, 67, 37–69. <https://doi.org/10.1007/BF01277501>
- Gray, W. M., Landsea, C. W., Mielke, P. W., & Berry, K. J. (1992). Predicting Atlantic seasonal hurricane activity 6–11 months in advance. *Weather and Forecasting*, 7, 440–455. [https://doi.org/10.1175/1520-0434\(1992\)007<0440:PASHAM.2.0.CO;2](https://doi.org/10.1175/1520-0434(1992)007<0440:PASHAM.2.0.CO;2)
- Harr, P. A., & Elsberry, R. L. (1991). Tropical cyclone track characteristics as a function of large-scale circulation anomalies. *Monthly Weather Review*, 119, 1448–1468. [https://doi.org/10.1175/1520-0493\(1991\)119<1448:TCTCAA.2.0.CO;2](https://doi.org/10.1175/1520-0493(1991)119<1448:TCTCAA.2.0.CO;2)
- He, Y., Sheng, Z., & He, M. (2020). Spectral analysis of gravity waves from near space high-resolution balloon data in northwest China. *Atmosphere*, 11, 133. <https://doi.org/10.3390/atmos11020133>
- Holland, G. J., & Lander, M. (1993). The meandering nature of tropical cyclone tracks. *Journal of the Atmospheric Sciences*, 50, 1254–1266. [https://doi.org/10.1175/1520-0469\(1993\)050<1254:TMNOTC.2.0.CO;2](https://doi.org/10.1175/1520-0469(1993)050<1254:TMNOTC.2.0.CO;2)
- Hong, C.-C., Li, Y.-H., Li, T., & Lee, M.-Y. (2011). Impacts of central Pacific and eastern Pacific El Niños on tropical cyclone tracks over the western North Pacific. *Geophysical Research Letters*, 38, L16712. <https://doi.org/10.1029/2011GL048821>
- Hu, F., Li, T., Liu, J., Bi, M., & Peng, M. (2018). Decrease of tropical cyclone genesis frequency in the western North Pacific since 1960s. *Dynamics of Atmospheres and Oceans*, 81, 42–50. <https://doi.org/10.1016/j.dynatmoce.2017.11.003>
- Kalnay, E., & coauthors (1996). The NCEP/NCAR 40-year reanalysis project. *Bulletin of the American Meteorological Society*, 77, 437–471. [https://doi.org/10.1175/1520-0477\(1996\)077<0437:TNYRP>2.0.CO;2](https://doi.org/10.1175/1520-0477(1996)077<0437:TNYRP>2.0.CO;2)
- Kim, D., Kim, H., Park, D. R., & Park, M. (2017). Variation of the tropical cyclone season start in the western North Pacific. *Journal of Climate*, 30, 3297–3302. <https://doi.org/10.1175/JCLI-D-16-0888.1>
- Klotzbach, P. J. (2007). Recent developments in statistical prediction of seasonal Atlantic basin tropical cyclone activity. *Tellus*, 59A, 511–518. <https://doi.org/10.1111/j.1600-0870.2007.00239.x>
- Kossin, J. P. (2018). A global slowdown of tropical-cyclone translation speed. *Nature*, 558(7708), 104–107. <https://doi.org/10.1038/s41586-018-0158-3>
- Kossin, J. P., Emanuel, K. A., & Camargo, S. J. (2016). Past and projected changes in western North Pacific tropical cyclone exposure. *Journal of Climate*, 25, 5725–5739. <https://doi.org/10.1175/jcli-d-16-0076.1>
- Kossin, J. P., Emanuel, K. A., & Vecchi, G. A. (2014). The poleward migration of the location of tropical cyclone maximum intensity. *Nature*, 509(7500), 349–352. <https://doi.org/10.1038/nature13278>
- LaRow, T. E., Stefanova, L., Shin, D.-W., & Cocks, S. (2010). Seasonal Atlantic tropical cyclone hindcasting/forecasting using two sea surface temperature datasets. *Geophysical Research Letters*, 37, L02804. <https://doi.org/10.1029/2009GL041459>
- Lee, C.-Y., Tippett, M. K., Sobel, A. H., & Camargo, S. J. (2018). An environmentally forced tropical cyclone hazard model. *Journal of Advances in Modeling Earth Systems*, 10, 233–241. <https://doi.org/10.1002/2017MS001186>
- Lehmiller, G. S., Kimberlain, T. B., & Elsner, J. B. (1997). Seasonal prediction models for North Atlantic basin hurricane location. *Monthly Weather Review*, 125, 1780–1791. [https://doi.org/10.1175/1520-0493\(1997\)125<1780:SPMFNA.2.0.CO;2](https://doi.org/10.1175/1520-0493(1997)125<1780:SPMFNA.2.0.CO;2)
- Li, R. C. Y., & Zhou, W. (2012). Changes in western Pacific tropical cyclones associated with the El Niño–southern oscillation cycle. *Journal of Climate*, 25, 5864–5878. <https://doi.org/10.1175/JCLI-D-11-00430.1>
- Lin, Y., Zhao, M., & Zhang, M. (2015). Tropical cyclone rainfall area controlled by relative sea surface temperature. *Nature Communications*, 6(1), 1–7. <https://doi.org/10.1038/ncomms7591>
- Liu, K. S., & Chan, J. C. L. (2008). Interdecadal variability of western North Pacific tropical cyclone tracks. *Journal of Climate*, 21, 4464–4476. <https://doi.org/10.1175/2008JCLI2207.1>
- Mantua, N. J., Hare, S. R., Zhang, Y., Wallace, J. M., & Francis, R. C. (1997). A Pacific Interdecadal Climate Oscillation with Impacts on Salmon Production. *Bulletin of the American Meteorological Society*, 78(6), 1069–1079. [https://doi.org/10.1175/1520-0477\(1997\)078<1069:co;2](https://doi.org/10.1175/1520-0477(1997)078<1069:co;2)
- Park, D.-S. R., Ho, C.-H., Kim, J.-H., & Kim, H.-S. (2011). Strong landfall typhoons in Korea and Japan in a recent decade. *Journal of Geophysical Research*, 116, D07105. <https://doi.org/10.1029/2010JD014801>
- Parker, D., et al. (2007). Decadal to multidecadal variability and the climate change background. *Journal of Geophysical Research*, 112, D18115. <https://doi.org/10.1029/2007JD00841>
- Patricola, C. M., Camargo, S. J., Saravanan, R., & Chang, P. (2018). The influence of ENSO flavors on western North Pacific tropical cyclone activity. *Journal of Climate*, 31, 5395–5416. <https://doi.org/10.1175/JCLI-D-17-0678.1>
- Peduzzi, P., Chatenoux, B., Dao, H., de Bono, A., Herold, C., Kossin, J., et al. (2012). Global trends in tropical cyclone risk. *Nature Climate Change*, 2, 289–294. <https://doi.org/10.1038/nclimate1410>
- Power, S., Casey, T., Folland, C. K., Colman, A., & Mehta, V. (1999). Inter-decadal modulation of the impact of ENSO on Australia. *Climate Dynamics*, 15, 319–323.
- Pudov, V. D., & Petrichenko, S. A. (2001). 1997–1998 El Niño and tropical cyclone genesis in the northwestern Pacific. *Izvestiya Atmospheric and Oceanic Physics*, 37, 576–583. <https://doi.org/10.1002/joc.617>
- Ramsay, H. A., & Sobel, A. H. (2011). Effects of relative and absolute sea surface temperature on tropical cyclone potential intensity using a single-column model. *Journal of Climate*, 24, 183–193. <https://doi.org/10.1175/2010JCLI3690.1>
- Rayner, N. A., Parker, D. E., Horton, E. B., Folland, C. K., Alexander, L. V., Rowell, D. P., et al. (2003). Global analyses of sea surface temperature, sea ice, and night marine air temperature since the late nineteenth century. *Journal of Geophysical Research*, 108, 4407. <https://doi.org/10.1029/2002jd002670>
- Riehl, H., & Shafer, R. J. (1944). The recurvature of tropical storms. *Journal of the Atmospheric Sciences*, 1, 42–54. [https://doi.org/10.1175/1520-0469\(1944\)001<0001:TROTS.2.0.CO;2](https://doi.org/10.1175/1520-0469(1944)001<0001:TROTS.2.0.CO;2)
- Shen, Y., Sun, Y., Camargo, S. J., & Zhong, Z. (2018). A quantitative method to evaluate tropical cyclone tracks in climate models. *Journal of Atmospheric and Oceanic Technology*, 35, 1807–1818. <https://doi.org/10.1175/JTECH-D-18-0056.1>
- Sheng, Z., Zhou, L., & He, Y. (2020). Retrieval and analysis of the strongest mixed layer in the troposphere. *Atmosphere*, 11, 264. <https://doi.org/10.3390/atmos11030264>
- Smith, T. M., & Reynolds, R. W. (2003). Extended reconstruction of global sea surface temperatures based on COADS data (1854–1997). *Journal of Climate*, 16, 1495–1510. <https://doi.org/10.1175/1520-0442-16.10.1495>

- Song, J., & Klotzbach, P. J. (2018). What has controlled the poleward migration of annual averaged location of tropical cyclone lifetime maximum intensity over the western North Pacific since 1961? *Geophysical Research Letters*, *45*, 1148–1156. <https://doi.org/10.1002/2017GL076883>
- Sun, Y., Zhong, Z., Li, T., Yi, L., Camargo, S. J., Hu, Y., et al. (2017a). Impact of ocean warming on tropical cyclone track over the western North Pacific: A numerical investigation based on two case studies. *Journal of Geophysical Research: Atmospheres*, *122*, 8617–8630. <https://doi.org/10.1002/2017JD026959>
- Sun, Y., Zhong, Z., Li, T., Yi, L., Hu, Y., Wan, H., et al. (2017b). Impact of ocean warming on tropical cyclone size and its destructiveness. *Scientific Reports*, *7*(1), 8154. <https://doi.org/10.1038/s41598-017-08533-6>
- Sun, Y., Zhong, Z., Li, T., et al. (2018). A recent reversal in the poleward shift of western North Pacific tropical cyclones. *Geophysical Research Letters*, *45*, 9944–9952. <https://doi.org/10.1029/2018GL079686>
- Sun, Y., Zhong, Z., Yi, L., Li, T., Chen, M., Wan, H., et al. (2015). Dependence of the relationship between the tropical cyclone track and western Pacific subtropical high intensity on initial storm size: A numerical investigation. *Journal of Geophysical Research: Atmospheres*, *120*, 11,451–11,467. <https://doi.org/10.1002/2015JD023716>
- Swanson, K. L. (2008). Nonlocality of Atlantic tropical cyclone intensities. *Geochemistry, Geophysics, Geosystems*, *9*, Q04V01. <https://doi.org/10.1029/2007GC001844>
- Tippett, M. K., Camargo, S. J., & Sobel, A. H. (2011). A Poisson regression index for tropical cyclone genesis and the role of large-scale vorticity in genesis. *Journal of Climate*, *21*, 2335–2357. <https://doi.org/10.1175/2010JCLI3811.1>
- Tu, S., Xu, F., & Xu, J. (2018). Regime shift in the destructiveness of tropical cyclones over the western North Pacific. *Environmental Research Letters*, *13*, 094021. <https://doi.org/10.1088/1748-9326/aade3a>
- Tuleya, R., Bender, M., & Kurihara, Y. (1984). A simulation study of the landfall of tropical cyclones using a movable nested mesh model. *Monthly Weather Review*, *112*, 124–136. [https://doi.org/10.1175/1520-0493\(1984\)112<0124:ASSOTL.2.0.CO;2](https://doi.org/10.1175/1520-0493(1984)112<0124:ASSOTL.2.0.CO;2)
- Vecchi, G. A., & Soden, B. J. (2007). Effect of remote sea surface temperature change on tropical cyclone potential intensity. *Nature*, *450*(7172), 1066–1070. <https://doi.org/10.1038/nature06423>
- Vecchi, G. A., Swanson, K. L., & Soden, B. J. (2008). Whither hurricane activity? *Science*, *322*, 687–689. <https://doi.org/10.1126/science.1164396>
- Wang, B., & Chan, J. C. L. (2002). How strong ENSO events affect tropical storm activity over the western North Pacific. *Journal of Climate*, *15*, 1643–1658. [https://doi.org/10.1175/1520-0442\(2002\)015<1643:HSEAT.2.0.CO;2](https://doi.org/10.1175/1520-0442(2002)015<1643:HSEAT.2.0.CO;2)
- Wang, B., Liu, J., Kim, H. J., et al. (2013). Northern Hemisphere summer monsoon intensified by mega-El Niño/Southern Oscillation and Atlantic multidecadal oscillation. *Proceedings of the National Academy of Sciences of the United States of America*, *110*, 5347–5352. <https://doi.org/10.1073/pnas.1219405110>
- Wang, H., Sun, J., & Fan, K. (2007). Relationships between the North Pacific Oscillation and the typhoon/hurricane frequencies. *Science China*, *50D*, 1409–1416. <https://doi.org/10.1007/s11430-007-0097-6>
- Watterson, I. G., Evans, J. L., & Ryan, B. F. (1995). Seasonal and interannual variability of tropical cyclogenesis: Diagnostics from large-scale fields. *Journal of Climate*, *8*, 3052–3066. [https://doi.org/10.1175/1520-0442\(1995\)008<3052:CO;2](https://doi.org/10.1175/1520-0442(1995)008<3052:CO;2)
- Webster, P. J., Magaña, V. O., Palmer, T. N., Shukla, J., Tomas, R. A., Yanai, M., & Yasunari, T. (1998). Monsoons: Processes, predictability, and the prospects for prediction. *Journal of Geophysical Research: Oceans*, *103*(C7), 14,451–14,510. <https://doi.org/10.1029/97jc02719>
- Wilks, D. S. (2006). *Statistical methods in the atmospheric sciences*, (2nd ed. p. 627). New York: Academic Press.
- Wu, L., & Wang, B. (2004). Assessing impacts of global warming on tropical cyclone tracks. *Journal of Climate*, *17*, 1686–1698.
- Wu, L., Wen, Z., & Huang, R. (2011). A primary study of the correlation between the net air-sea heat flux and the interannual variation of western North Pacific tropical cyclone track and intensity. *Acta Oceanologica Sinica*, *30*, 27–35.
- Wu, L., Wen, Z., Huang, R., & Wu, R. (2012). Possible linkage between the monsoon trough variability and the tropical cyclone activity over the western North Pacific. *Monthly Weather Review*, *140*, 140–150.
- Wu, M., Chang, W., & Leung, W. (2004). Impacts of El Niño–Southern Oscillation events on tropical cyclone landfalling activity in the western North Pacific. *Journal of Climate*, *17*, 1419–1428. [https://doi.org/10.1175/1520-0442\(2004\)017<1419:IOENOE.2.0.CO;2](https://doi.org/10.1175/1520-0442(2004)017<1419:IOENOE.2.0.CO;2)
- Zhang, Q., Liu, Q., & Wu, L. (2009). Tropical cyclone damages in China 1983–2006. *Bulletin of the American Meteorological Society*, *90*, 489–495. <https://doi.org/10.1175/2008BAMS2631.1>
- Zhang, W., Graf, H. F., Leung, Y., & Herzog, M. (2012). Different El Niño types and tropical cyclone landfall in East Asia. *Journal of Climate*, *25*, 6510–6523. <https://doi.org/10.1175/JCLI-D-11-00488.1>
- Zhang, W., Leung, Y., & Fraedrich, K. (2015). Different El Niño types and intense typhoons in the western North Pacific. *Climate Dynamics*, *44*(11–12), 2965–2977. <https://doi.org/10.1007/s00382-014-2446-4>
- Zhang, W., Vecchi, G. A., Murakami, H., et al. (2016). Improved simulation of tropical cyclone responses to ENSO in the western North Pacific in the high-resolution GFDL HiFLOR coupled climate model. *Journal of Climate*, *29*, 1391–1415. <https://doi.org/10.1175/JCLI-D-15-0475.1>
- Zhao, X. R., Sheng, Z., Li, J. W., Yu, H., & Wei, K. J. (2019). Determination of the “wave turbopause” using a numerical differentiation method. *Journal of Geophysical Research: Atmospheres*, *124*, 10,592–10,607. <https://doi.org/10.1029/2019JD030754>
- Zhou, W., & Chan, J. C. L. (2007). ENSO and the South China Sea summer monsoon onset. *International Journal of Climatology*, *27*, 157–167. <https://doi.org/10.1002/joc.1380>